



3D-Printed micro-optofluidic device for chemical fluids and cells detection

Fabiana Cairone¹ · Santi Davi¹ · Giovanna Stella¹ · Francesca Guarino² · Giuseppe Recca³ · Gianluca Cicala⁴ · Maide Bucolo¹

Published online: 18 May 2020
© Springer Science+Business Media, LLC, part of Springer Nature 2020

Abstract

In this work, it is presented a micro-optofluidic flow detector used for on-chip biological and chemical samples investigation. It is made in Poly-dimethyl-siloxane using a master-slave approach based on the *3D-Printing* techniques. The micro-optofluidic device is made by assembling a microfluidic T-junction with a micro-optical section that consists of two optical fiber insertions and a PDMS gold-spattered micro-waveguide. The working principle in the detection is based on a different light transmission correlated to the fluid interfering with the laser beam in a micro-channel section. The proposed solution allows to realize a PDMS micro-device taking the advantage of *3D-Printing* and goes beyond the restriction in the material selection. The device's performances were tested in the fluids detection and in the evaluation of the cell concentrations. Additionally, the micro-device was used as a real-time two-phase fluids flow detector. The two-phases flows were successfully monitored in different experimental conditions, varying both hydrodynamic and optical external stimuli.

Keywords Microfluidics · Micro-optics · Two-phase flow · Real-time monitoring · Laser-fluid interaction

1 Introduction

Two-phase microfluidics processes, generated by two immiscible fluids or micro-particles dispersed in a fluid with a certain concentration, are common in many biological,

chemical and medical researches (Li 2006). The choice of methodologies and technologies for the detection and control of biological and chemical fluids in micro-channels is a crucial issue in the design of highly complex micro-systems for Lab-on-a-Chip applications (Bucolo et al. 2017; Walsh et al. 2017).

Among all the technologies, the optical one offers the advantages of a wide range of measurement options being minimally invasive (Minzioni et al. 2017). In this context, the trend is to move from the bench equipment used to perform the standard optical detection procedures based on fluorescence, absorbance, infrared, chemiluminescence to their miniaturization in a single portable low-cost device (Brammer and Mappes 2010; Yeshaiahu et al. 2010). The studies for the realization of micro-optofluidic devices where optical and fluidic components are miniaturized and integrated into a single chip move in this direction (Cairone et al. 2016a; Cong et al. 2019; Yamaguchi et al. 2016; Zhao et al. 2019).

In the fabrication of micro-optofluidic devices two aspects that have a central role, being strictly correlated, are: the material selection and the fabrication method (Becker and Locascio 2002).

In this work, it is presented a micro-optofluidic flow detector realized in Poly-dimethyl-siloxane (PDMS) using a master-slave approach based on the *3D-Printing* technique.

✉ Maide Bucolo
maide.bucolo@unict.it

Francesca Guarino
fguarin@unict.it

Giuseppe Recca
giuseppe.recca@cnr.it

Gianluca Cicala
gcicala@unict.it

- ¹ Department of Electrical Electronic and Computer Science Engineering, University of Catania, viale A. Doria 6, 95125 Catania, CT, Italy
- ² Department of Biomedical and Biotechnological Science, University of Catania, viale A. Doria 6, 95125 Catania, CT, Italy
- ³ National Research Council of Italy - IPCB Institute for Polymers, Composites and Biomaterials, via Gaifami 18, 95126 Catania, CT, Italy
- ⁴ Department of Civil Engineering and Architecture, University of Catania, viale A. Doria 6, 95125 Catania, CT, Italy

The widely used technique for rapid prototyping of PDMS micro-devices is Soft-lithography (McDonald and Whitesides 2002; Ng et al. 2007). It combines a good resolution, up few micrometers, with the advantages of the PDMS properties as: bio-compatibility, optical transparency, impermeability to liquids and high chemical resistance. The literature gives different evidence on the use of this technology for micro-optical components realization (Camou et al. 2003; Chang-Yen et al. 2005; Llobera et al. 2008) and their applications for microfluidic processes monitoring (Sapuppo et al. 2010, 2012).

Although up to now, professional inkjet *3D-Printer* cannot compete with the resolution obtained by Soft-lithography, satisfactory results are shown with micro-structures up to 300 μm . A wide range of micro-devices examples and fabrication protocols have been presented in literature to exploit fully the potential and limitations of this technology (Au et al. 2016; Bhattacharjee et al. 2016; Macdonald et al. 2017). The recent trend is the one-step direct *3D-Printing* of the micro-devices (Chan et al. 2015).

The challenge to extend *3D-Printing* in making micro-optofluidic chips has given rise to the need for specific optical properties of the materials. Nowadays, PDMS is not readily available for printing on inkjet machines. Most of the inkjet *3D-Printers* use cytotoxic or non-transparent materials. Nevertheless, the arising of different Lab-on-a-Chip applications (Yazdi et al. 2016; Chan et al. 2017), to date no-material with both features necessary in the design of the micro-optofluidic chips, as the bio-compatibility and the optical transparency, are available (Weisgrab et al. 2019).

The master-slave solution presented aims to overcome these limitations and to extend the use of the *3D-Printing* in the realization of micro-optical components, going beyond the restriction in the material selection.

In Cairone et al. (2016a), we have presented a PDMS micro-optofluidic device, realized by the master-slave *3D-Printing* approach, to drive a laser light beam toward a microfluidic channel and to detect a two-phase flow. In this work, we expand this scope of investigation both by embedding in the designed chip a gold-sputtering micro-waveguide and by testing its performance to detect different samples and to track in real-time fluids flows. This detection approach, as suitable solution for on-chip device analysis avoiding bulky and costly equipment, was successfully implemented in our recent works to characterize the Red Blood Cells (Cairone et al. 2018a, b) and slug flows in micro-channels (Cairone et al. 2016b; Gagliano et al. 2020). That offers, technologically, a greater flexibility in the design ensuring to deliver as close as possible to the sample the laser light and, methodologically, the opportunity to widen its use in a variety of biological and chemical Lab-on-a-Chip applications. Indeed, having the opportunity to steer

the laser light with power below 100mW opens to a wide variety of measurements (Cong et al. 2019; Cossarizza et al. 2017).

The paper is organized as follows. Section 2 describes the PDMS micro-optofluidic device design and realization by the proposed master-slave solution based on the *3D-Printing* techniques. A T-junction micro-channel was integrated with a micro-optical section that consists of two optical fiber insertions and a micro-waveguide. Ray tracing simulations were used in the optimization of the micro-optical section design, and a specific procedure was developed for the assembling of the micro-fluidic and micro-optical components. In Section 3, the results obtained experimentally in both chemical and biological contexts are presented and discussed. The micro-optofluidic detector realized was then successfully tested for the differentiation of chemical fluids and cell suspension concentrations. Additionally, the detector was tested for real-time monitoring of two-phase flows in slug regime.

2 Micro-optofluidic detector design and realization

The micro-optofluidic detector was designed to be a compact device that integrates the micro-optic and micro-fluidic components. In Fig. 1 a cartoon of the working principle is presented: assuming that two fluids with quite different refraction indices flow in a micro-channel, and an incident laser beam interferes with them in a specific micro-channel area. It is possible to obtain a different light transmission based on which fluid is interfering with the laser beam at that moment.

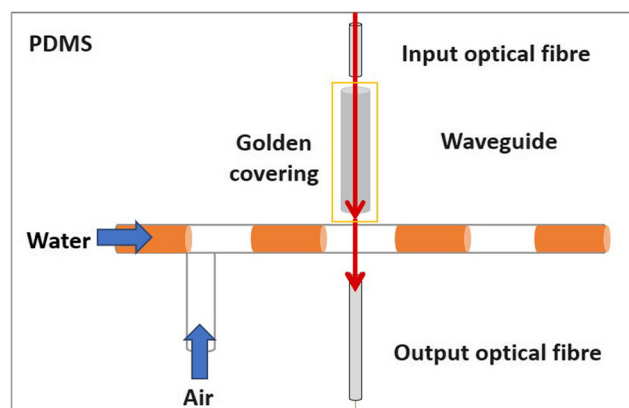
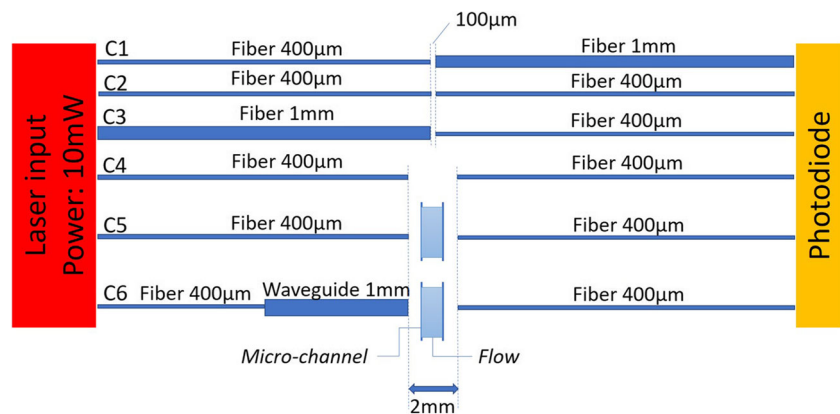


Fig. 1 Working principle of micro-optofluidic flow detector. The microfluidic component consists of a T-junction micro-channel. The micro-optical section of the device is orthogonal to the straight part of the micro-channel and includes two optical fiber insertions and a waveguide

Fig. 2 The six alignment configurations considered for the micro-optical section optimization: {C1, C2, C3, C4} in absence of a fluid, C5 in presence of a fluid and C6 with the integration of the PDMS micro-waveguide



The microfluidic component consists of a T-junction micro-channel. Two different fluids or a particle suspension can be injected by the two inlets, if necessary having one plugged (see Fig. 1).

The optical section of the device is orthogonal to the straight part of the micro-channel at a distance of 15 mm from the T-junction to assure the flow stability. It includes two optical fiber insertions and a waveguide allocation area. The PDMS waveguide was realized separately and shielded by a material with a refractive index lower than the one of the PDMS. Thanks to the first optical fiber insertion, the laser light is conveyed to the PDMS waveguide and then reaches the area of the micro-channel investigated. The light travels to the sample, and it is detected by a second optical fiber aligned at the opposite side of the micro-channel. The optical signal acquired is then correlated to the flow inside the micro-channel. To finalize the design, the ray-tracing simulations of the optical section were carried out considering the conditions of presence and absence of the flow in-between the micro-optical components aligned on the opposite sides of the micro-channel.

2.1 Micro-optical section optimization

The performances of the micro-optical section were evaluated by the ray-tracing simulations using TracePro. Six alignment configurations were considered: the first four {C1, C2, C3, C4} to study the micro-optical components alignment, and the other two {C5, C6} for the characterization in presence of a fluid. A laser light source with a power intensity of 10 mW (100 rays per area) was set. The model of the optical fibers (SMA to free end) developed in Cairone et al. (2016a) was used. In Fig. 2 the six simulated conditions are sketched.

The configurations {C1, C2} were taken into account to determine the optimal core diameter of the output optical fiber. Two diameters were investigated 1 mm and 400 µm. The laser source coupled with the input optical fiber (core

of 400 µm) was aligned at a distance of 100 µm with the output optical fiber coupled with the acquisition system.

The configurations {C2, C3} were used to determine the optimal core diameter of the input optical fiber, using 400 µm and 1 mm. In both cases, the input optical fiber coupled with the laser source was aligned at a distance of 100 µm with the output optical fiber (core of 400 µm).

The percentage of incident rays on the output optical fiber was detected by the irradiation map. The best performance was obtained in the configurations {C1, C2} with respectively {0 – 26}% of losses. A lost of 84% was in configuration C3, underling that a diameter of the transmission-fiber equal or smaller than the one of the receiving fiber reduces the light-lost.

In the configuration C4, it was used the same input-output optical fibers set-up of C2 increasing the alignment distance up to 2 mm, space necessary for the micro-channel insertion. The losses increase to a percentage of 66%.

In the configuration C5, a micro-channel of 1 mm depth filled by a fluid was inserted in-between the optical fibers. Finally, in the configuration C6 a PDMS waveguide was aligned to the input optical fiber, as in the design of flow detector realized.

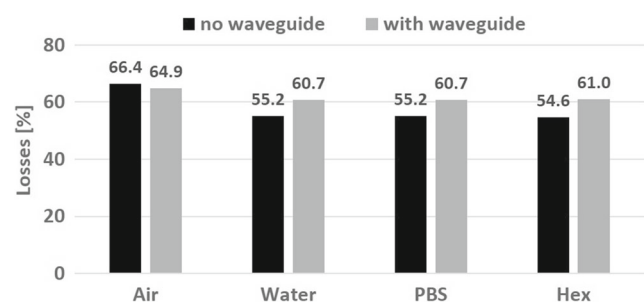
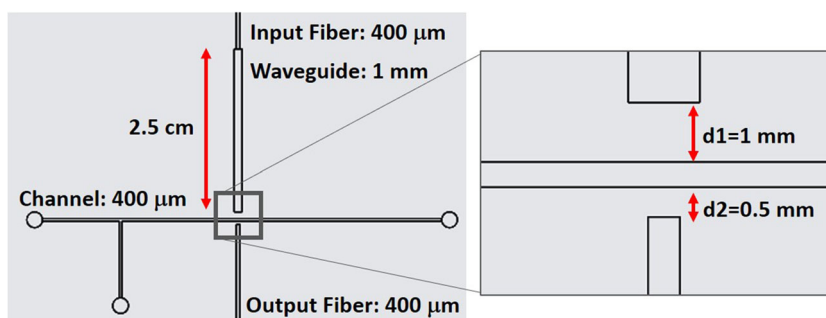


Fig. 3 Performance of the micro-optical section by ray-tracing simulations. In the bar histogram, the losses in the output optical fiber in percentage for the configurations {C5, C6} are compared in presence of {Air, Water, PBS, Hex}

Fig. 4 Details in the design of the micro-optofluidics detector: the micro-channel, two sections for the optical fiber insertions and the allocation area for the waveguide



In the configurations {C5, C6}, four fluids were considered {Air, Water, Phosphate-Buffered saline (labeled PBS) and Hexadecane (labeled Hex)} with different refractive indices respectively, $n_{fluid} \in \{1, 1.33, 1.34, 1.434\}$. As expected, the greater losses are computed for the Air. Additionally, the slight differentiation among Water, PBS, Hex is consistent with the slight difference in their refraction indices. In Fig. 3, a bar histogram compares the losses in {C5, C6} per fluid. It is worth to notice that the insertion of the PDMS micro-waveguide does not alter significantly the performance.

2.2 3D-Printing fabrication process PDMS-based

The design of the micro-optofluidic detector was established based on a trade-off among the results of the ray-tracing simulations, the material (PDMS) and the fabrication technology (3D-Printing) selected. All the details are reported in Fig. 4.

Two final computer designs (CADs) were realized one for the micro-system, which includes the micro-channel and the micro-optical section, and one for the micro-waveguide. A procedure to assemble those in an embedded device was also established.

The micro-channel has a squared section of $400 \mu\text{m}$ side. The diameter of the inlets and outlet wells is 2.4 mm . The T-junction is at a distance of 13 mm from the inlets and

of 15 mm from the micro-channel area investigated. The optical section includes two optical fiber insertions and a waveguide allocation. The following constrains were taken into account:

- the diameter of the PDMS waveguide was set to 1 mm due to 3D-Printing limitation;
- the distances between micro-optical section at the two sides of the micro-channel were set to $d_1 = 1 \text{ mm}$, $d_2 = 0.5 \text{ mm}$, to ensure a safety bounding and avoid the fluid leakage;
- the diameter of the output optical fiber was set equal to the micro-channel width $400 \mu\text{m}$ to maximize the acquisition.

In a waveguide, the light travels inside a channel made with a material whose refractive index has to be greater than that of the surrounding material to cause the total reflection phenomena. In this case, the PDMS waveguide ($n_1 = 1.41$) was shielded by gold ($n_{Au} = 0.47$) and placed in the PDMS allocation area of the micro-system. The square waveguide was realized with a width of 1 mm and a length of 2.5 cm .

Being still not possible to realize directly PDMS device with the 3D-Printer, a specific master-slave procedure was used for both the micro-system and the waveguide. The two CADs were printed using a photo-sensitive resin, and their surfaces treated to avoid any type of reticulation of the resin in contact with the PDMS. In our previous work (Cairone

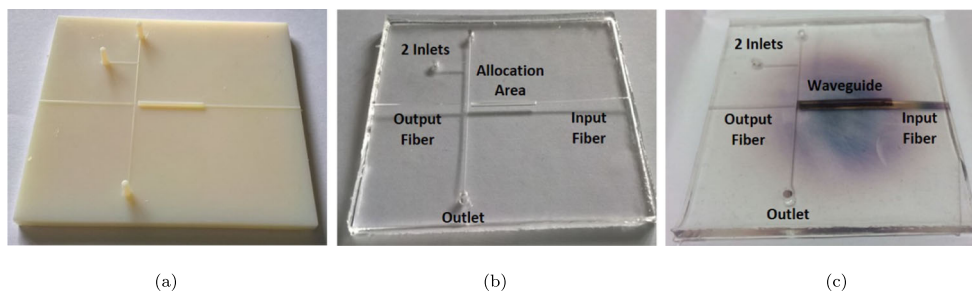


Fig. 5 3D-Printing PDMS-based steps of the protocol to assemble the micro-optofluidic detector. **a** The mold of the micro-system which includes the micro-channel and the micro-optical section. **b** The

casted micro-system realized in PDMS. **c** The complete PDMS micro-optofluidic device with the allocation area where the gold-spattered micro-waveguide is inserted

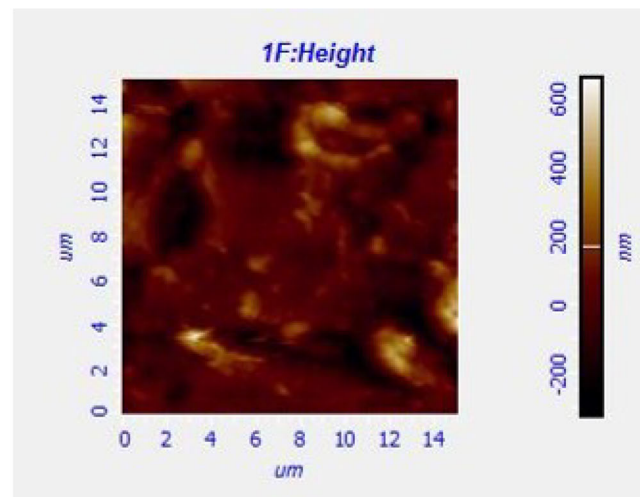
et al. 2016a), a chemical treatment was adopted, here a further improvement was reached thanks to the UV-based illumination.

The master-slave mold was printed by using an inkjet printer model Objet260 Connex1, Stratasys (Rheinmünster, Germany). The material used for the mold was the VeroWhitePlus, and the FullCure705 as support. The support material is removable with water and commonly used for printing hollow parts. The Object260 printer is a professional inkjet, its use consolidated and the precision range stated by the producers (<https://www.stratasys.com/3d-printers/objet-260-500-connex1>). The horizontal layer thickness can be as fine as $16\ \mu\text{m}$. Due to the layer-by-layer construction, the resolution and surface quality depends on the build orientation of the part. To reach a trade-off between the printing speed and the mold resolution, a flat orientation was set with $50\ \mu\text{m}$ layer-by-layer thickness. The printing time for the micro-system mold, shown in Fig. 5a, was 15 hr.

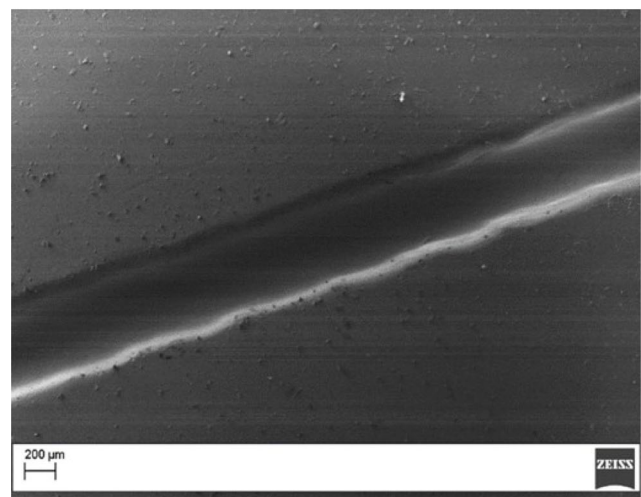
In the following phase, the silicone and the curing agent of PDMS (Sylgard 184 elastomer kit, Dow Corning) were mixed together according to the proportion (10 : 1) for the device layer (micro-systems and waveguide) and to the proportion of (5 : 1) for the bulk cover layer. After the degassing, the PDMS was poured in the two masters and placed in an oven at $50\ ^\circ\text{C}$ for 24 hours. Finally, the PDMS devices of the micro-system and the PDMS waveguide were peeled from their masters. The waveguide was gold-sputtered up to a thickness of $20\ \text{nm}$ using an Emitech K-550 sputter coater (Ashford Kent, UK). For assembling the device, the waveguide gold-sputtered was placed in the allocation area of the PDMS micro-system (see Fig. 5b) and the device bounded with a $0.5\ \text{mm}$ thick bulk by a reversible bound procedure. The complete micro-optofluidic detector is presented in Fig. 5c.

To test the precision of the 3D-Printed mold, its surface was analyzed by an Atomic Force Microscopy (AFM, NTEGRA by NT-MDT). The AFM measurements were carried out in different locations. As an example, in Fig. 6a the colormap of the roughness distribution in a square surface of $0.014\ \mu\text{m}$ side is shown, the colorbar reports the surface height in the range $[-0.5; 0.5]\ \mu\text{m}$. The average roughness measured in the mold was $(0.1 \pm 0.02)\ \mu\text{m}$.

To assess the precision of the casted PDMS device, its surface was analyzed with an EVO Scanning Electron Microscope (EVO-SEM, Zeiss). As an example, in Fig. 6b the SEM photo of a PDMS micro-channel section is reported. It is visible a minor undulation on the order below $0.1\ \mu\text{m}$ due probably to PDMS shrinkage. These results confirm that the device, realized with the presented master-slave approach, lies well in the resolution above $200\ \mu\text{m}$, so comparable with the values given in Weisgrab et al. (2019) using the direct 3D-Printing.



(a)

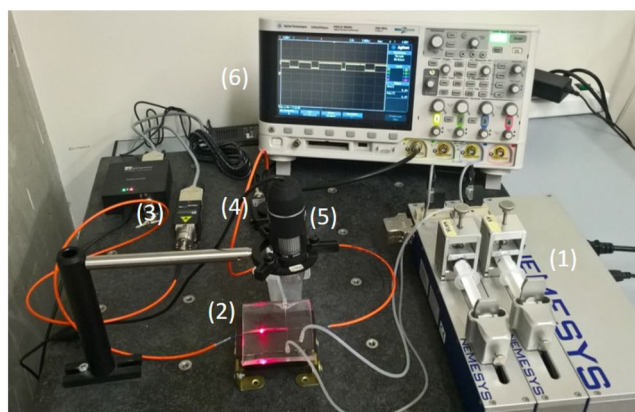


(b)

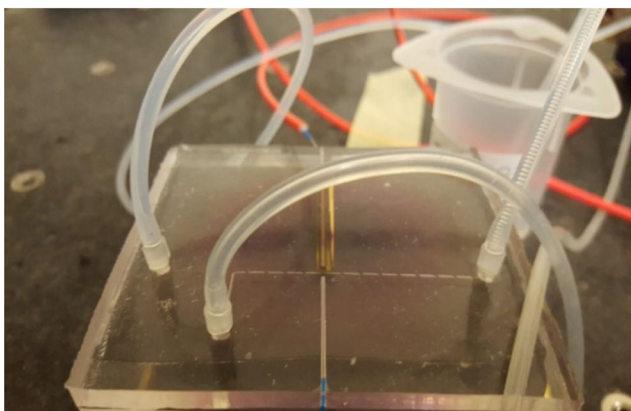
Fig. 6 **a** The roughness distribution in a square surface of $0.014\ \mu\text{m}$ side of the 3D-Printed mold, the colorbar reports the surface height in the range $[-0.5; 0.5]\ \mu\text{m}$. **b** The SEM photo of a micro-channel section of the casted PDMS device

3 Experimental results and discussion

The setup for the characterization of the micro-optofluidic flow detector is shown in Fig. 7a. Two multi-mode optical fibers with $N.A. = 0.22$ were used (SMA to free-end by Thorlabs) with a core diameter of $365 \pm 14\ \mu\text{m}$. The free-end of input optical fiber was clamped onto the device's input-fiber insertion, while the SMA-end was connected to the laser source (Rgb NovaPro Laser 660-125, wavelength used $660\ \text{nm}$). The second optical fiber was clamped by the free-end onto the device's output-fiber insertion and coupled by the SMA-end with a photodiode (PDA 100A, Thorlabs, gain used $50\ \text{dB}$). The signal received by the photodiode was acquired by an oscilloscope (Agilent



(a)



(b)

Fig. 7 **a** The setup for the characterization of the micro-optofluidic detector: (1) the syringe pumps, (2) the micro-device, (3) the laser source, (4) the photodiode, (5) the CCD, (6) the oscilloscope. **b** Zoom on the micro-optofluidic detector connected with the inlet and outlet tubes and the two optical fibers

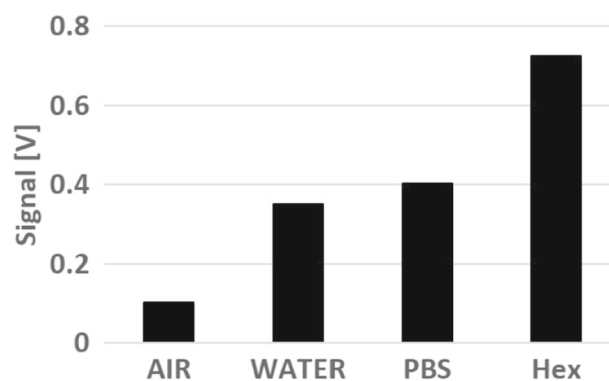
MSO7054A) with a sampling frequency of 500 Hz. For a visual inspection of the process, a digital USB microscope with direct illumination was placed above the device. A pair of syringe pumps (neNESYS by Cetoni GmbH) was used to generate a controlled flow into micro-channel. The picture of the micro-optofluidic detector connected with the inlet and outlet tubes and the two optical fibers is shown in Fig. 7b.

The performances of the micro-optofluidic detector were tested in both chemical and biological contexts. Initially, two experimental campaigns were carried out to investigate the device's ability in the fluids differentiation {Air, Water, PBS, Hex} and in the evaluation of the cell suspension concentrations. In the third experimental campaign, the micro-device was tested as a real-time slug flow detector.

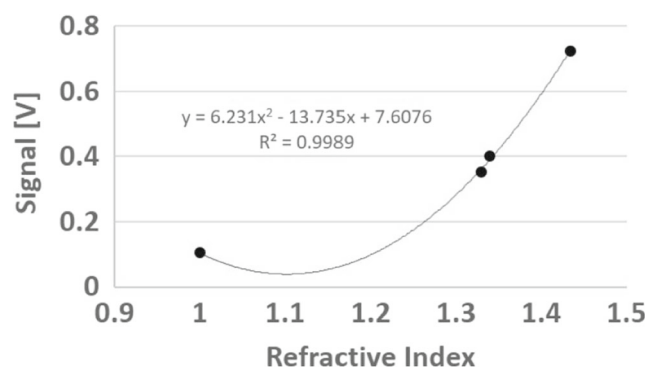
3.1 Detection of fluids and cell concentrations

Initially, to test the device's ability in fluids differentiation, a single flow of the fluids {Air, Water, PBS, Hex} were considered. One inlet of the T-junction was plugged and the other fed by a fluid with an input flow rate of 0.2 ml/min. A laser source with power of 1 mW was used.

The amplitude of the signal acquired by the oscilloscope (in [V]) for 10 s per each experimental condition was reported in the bar histograms in Fig. 8a–b. No significant variation was detected during the registrations, so no error bar was reported. Figure 8a evidences as the signal amplitude increases (and the relative losses decrease) at the increase of the fluid refractive index $n_{air} = 1$, $n_{water} = 1.33$, $n_{PBS} = 1.34$ and $n_{Hex} = 1.434$. A great sensitivity to the fluid changes can be noticed in the experimental results compared with that obtained in simulations, possibly due



(a)



(b)

Fig. 8 **a** Histogram of the signal amplitude acquired by the oscilloscope (in [V]) for the fluids considered {Air, Water, PBS, Hex}. **b** Calibration curve obtained by plotting per fluid the amplitude of the acquired signal versus the refraction index

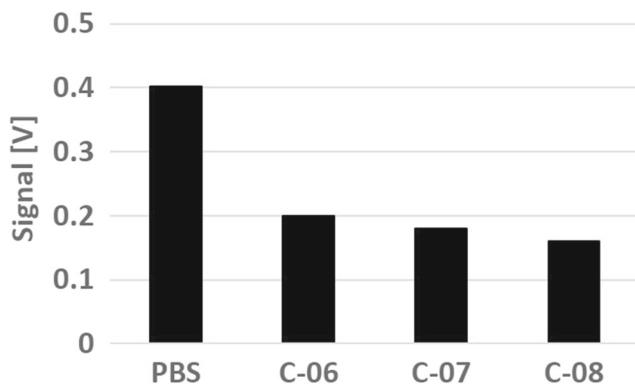


Fig. 9 Histogram of the signal amplitude acquired by the oscilloscope (in [V]) for the detection of the three Yeast cells concentrations in PBS suspension considered {C - 06, C - 07, C - 08}

to the limit of the ray-tracing in reproducing the fluid-laser interaction at the micro-channel boundaries.

The Fig. 8b plots per fluid the amplitude of the signal acquired (in [V]) versus the refraction index. The parabolic interpolation was also presented as an optimal data calibration.

In the second experimental campaign, one inlet of the T-junction was plugged and the other fed by a suspension of Yeast cells (*Saccharomyces Cerevisiae*) in PBS. A slow pulsatile pressure was applied. The Yeast cells were cultivated *in vitro* and then diluted in 10 ml of PBS to have three different concentrations $\{10^6, 10^7, 10^8\}$, labeled respectively {C - 06, C - 07, C - 08}. A laser source with power intensity of 1mW was used.

Also in the case of cell suspensions, it was possible to detect a variation in the amplitude of the acquired signals (in [V]), as shown in Fig. 9. The signal amplitude decrease at the concentration increase can be correlated with the dispersion of light for the presence of a greater number of particles. In this case, a less sensitivity of the detector can be observed. That will be investigated in the future development by using lower concentrations, different laser wavelengths and smaller micro-channel diameters.

3.2 Real-time detection of slug flows

In the third campaign, 24 experiments were carried out to evaluate the sensitivity of the micro-optofluidic device in real-time detection of two-phase flows. Three combinations of the immiscible fluids previously classified {Air, Water, PBS, Hex} were considered in their slug regime (Cairone et al. 2016b) as follows:

- Air-Water flow;
- Air-PBS flow;

Table 1 The nine combinations of the hydrodynamic (two input fluids flow-rates) and optical (laser power intensity) external stimuli used for the three considered slug flows

	Power (mW)	V_{air} (ml/min)	V_{lq} (ml/min)
Exp-1	1 - 5 - 10	0.1	0.2
Exp-2	1 - 5 - 10	0.15	0.3
Exp-3	1 - 5 - 10	0.2	0.4

- Air-Hex flow.

Both hydrodynamic and optical external stimuli were varied for a total of 9 combinations as summarized in Table 1. The hydrodynamic force was set using three values of the Air input flow rate (V_{air}), and doubling these for the selected liquid input flow rate {Air, Water, PBS, Hex} (V_{lq}), as follows:

- Exp-1: $\{V_{air} = 0.1 \text{ ml/min}, V_{lq} = 0.2 \text{ ml/min}\}$;
- Exp-2: $\{V_{air} = 0.15 \text{ ml/min}, V_{lq} = 0.3 \text{ ml/min}\}$;
- Exp-3: $\{V_{air} = 0.2 \text{ ml/min}, V_{lq} = 0.4 \text{ ml/min}\}$.

The Exp-3 for Air-Hex was excluded due to the excess of fluid leakage.

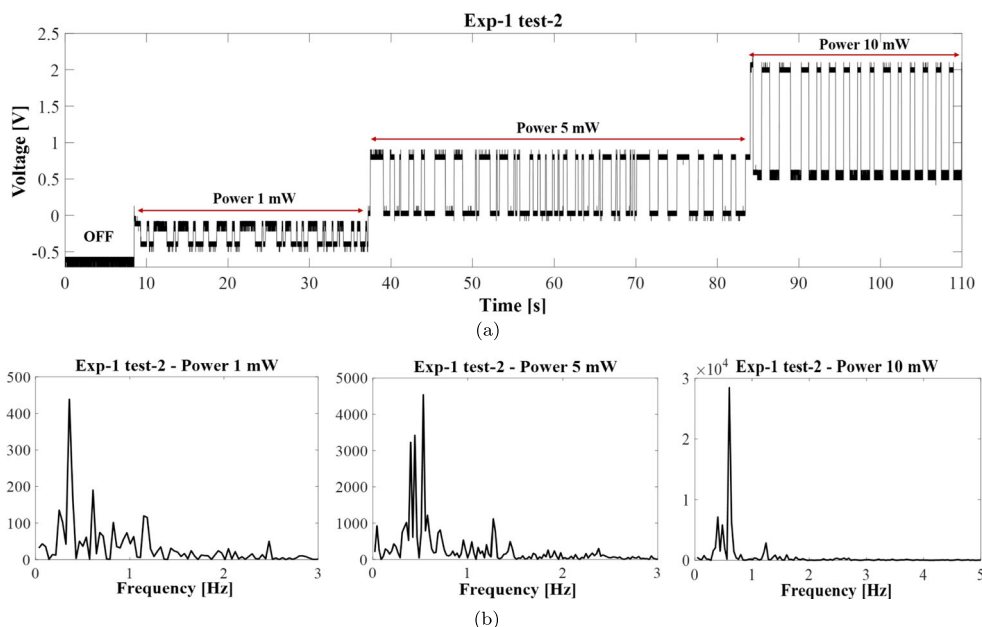
The laser light was set using three levels of the power intensity $\in \{1, 5, 10\}$ mW. The laser was turned on after 10 s and then its power was increased in the set $\in \{1, 5, 10\}$ mW during three time intervals. The same power intensity was maintained for around 35 s.

In Fig. 10a, as an example, it is plotted the optical signal acquired for the Air-Water flow in the Exp - 2; the three time windows were pointed. The signal shows a square-wave trend, whose increase of the average levels is correlated with the laser power intensity. The square-wave dynamics is due to the different light absorption at the passage of the fluids: the lower value is for the Air and the higher for the Water (Cairone et al. 2016b).

The eight signals acquired were segmented in three time intervals, per power intensity, and then processed both in time and frequency domain to characterize the fluids-laser interaction in the micro-channel.

Initially, the signals were processed to evaluate the average amplitude (in [V]) of the signal at the passage of each fluid {Air, Water, PBS, Hex} per laser power. In Fig. 11, it is reported the average of the signal amplitude per fluid obtained combining their values at different input flow rate conditions {Exp - 1, Exp - 2, Exp - 3} for the same laser power intensity. The error bars represent the range of these variations that, being negligible, confirm the consistency in the fluid detection during a dynamical acquisition increasing the pressure at the inlet. Furthermore, it is possible to evidence the sensitivity of the amplitude per

Fig. 10 The detected signal and the three spectra obtained for the *Air-Water* slug flow in the experimental condition *Exp - 2* ($V_{air} = 0.15 \text{ ml/min}$ and $V_{lq} = 0.3 \text{ ml/min}$). **a** The acquired optical signal trend, correlated with the air-water presence in the micro-channel area inspected. **b** The three spectra obtained by the signal segmentation in the three time intervals with the light power set to $\in \{1, 5, 10\} \text{ mW}$



fluid at the laser power $\in \{1, 5, 10\} \text{ mW}$. The amplitude is lower for the *Air* and then rises for the $\{Water, PBS, Hex\}$ in accordance with the results discussed in the previous Section.

Then, in Fig. 12, the ranges of variation per fluids pair $\{Air-Water, Air-PBS, Air-Hex\}$ and per power level were reported. The difference in the amplitude values obtained per fluid $\{Water, PBS, Hex\}$ were computed respect the amplitude value of the *Air*. The error bars sum the errors per fluid-pair. The results show an increase of the signal range per laser level, that leads to an improvement in fluids differentiation during the slugs passage. The enhancement is quite impressive in the case of *Air-Hex* flow: the signal range for the laser intensity of 10 mW is four times bigger than for 1 mW . This effect can be correlated with decreasing in the medium absorption induced by the density reduction at the temperature increase.

Finally, the signals segmented per power intensity were processed in the spectral domain to extract the dominant

frequency of the *Air/Fluid* slug passage. As an example, Fig. 10b reports the three spectra obtained per power $\in \{1, 5, 10\} \text{ mW}$ for the *Air-Water* flow in *Exp - 2*. The frequency peak is associated with the mean inter-distance of the two fluids sequence *Air-Liquid* inside the micro-channel (Cairone et al. 2016b; Gagliano et al. 2020).

The dominant peaks are reported in the bar histogram of Fig. 13. In Fig. 13a, no-significant frequency increases can be noticed by the fluid-laser interaction for both the $\{Air-Water, Air-PBS\}$ in *Exp - 1*. Then for the *Air-Water* slug flow a clear speed-up of the process was detected in the $\{Exp - 2, Exp - 3\}$. In the *Air-PBS* slug flow the acceleration is visible in *Exp - 2* for the laser power in $\{1, 5\} \text{ mW}$ and no-significant frequency change is in the *Exp - 3*.

Conversely in Fig. 13b, for the *Air-Hex* slug flow, the air-fluid sequence is faster than in the other fluid-pair conditions, the laser activation induces a visible slow-down

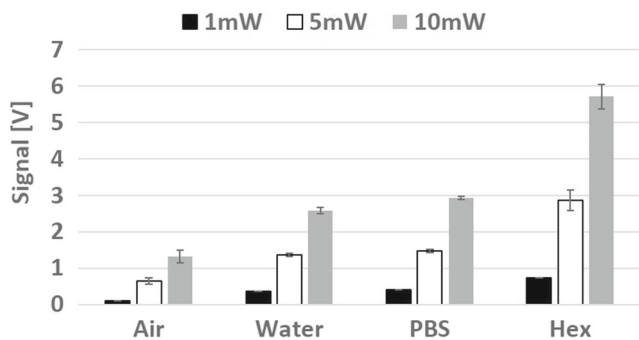


Fig. 11 The average amplitude of signals in [V] per fluid $\{Air, Water, PBS, Hex\}$ and per power intensity $\{1, 5, 10\} \text{ mW}$

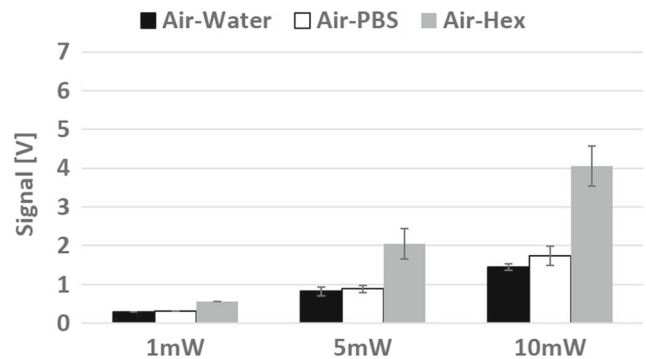


Fig. 12 The average range of the signal in [V] per fluid combinations $\{Air-Water, Air-PBS, Air-Hex\}$ and per power intensity $\{1, 5, 10\} \text{ mW}$

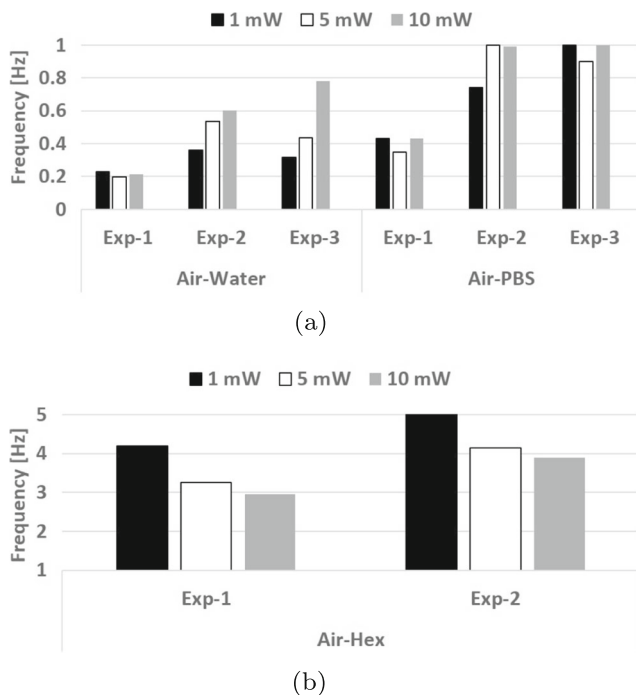


Fig. 13 Bar histograms of the dominant frequencies in the spectra for all the 24 experimental conditions. **a** {Air-Water, Air-PBS} **b** Air-Hex

of the process. Possibly this nonlinear phenomenon can be associated with an interlaced effect in the fluid-pair, due to their relative changes in their properties (as density and viscosity). After a certain power level seems that, due to the laser heating up, the process is slow-down by the dominance of the slower fluid *Air*.

4 Conclusions

In this work, it is presented a micro-optofluidic flow detector used for on-chip biological and chemical samples investigation. It was realized in PDMS using a master-slave solution based on the *3D-Printing* technique.

The *3D-Printing* technology is a promising fabrication process for the realization of a low-cost complex structure in this field, but to date, it is not possible the direct use of PDMS. The master-slave procedure, developed by the authors in Cairone et al. (2016a), has allowed to realize a PDMS micro-device of around 16 cm^2 , where micro-optical and microfluidic components were embedded. From one side, to produce a *3D-Printed* chip, with professional inkjet, can be time consuming and costly. On the other hand, the casting procedure, resembling that used in the Soft-lithography, is not complex and low-cost. Then using the same *3D-Printed* mold for multiple casting spreads its cost on several manufactured devices, being also advantageous for the chip production industrialization.

The micro-optofluidic flow detector is a compact device realized by assembling a microfluidic T-junction with a micro-optical section that consists of two optical fiber insertions and a micro-waveguide. The working principle of the micro-detector is based on the difference of the refraction indices of the fluids and particles that flow in the micro-channel. Its performances were tested in the fluids detection and in the evaluation of the cell concentrations. Additionally, the micro-device was used as a real-time two-phase slug flow detector in different experimental conditions, varying both hydrodynamic and optical external stimuli. The data collected from the micro-optofluidic device was additionally used to study the fluid-laser interaction in the micro-channel.

In the future developments, a further effort will put to the increase of the device sensitivity in cells differentiation. It will be widen the variety of cell suspensions and the concentrations to fully check its ability to be used in biological applications. That will offer, technologically, a greater flexibility in the design ensuring to deliver as close as possible to the sample the laser light and, methodologically, the opportunity to widen its use in a variety of biological and chemical Lab-on-a-Chip applications.

References

- A.K. Au, W. Huynh, L.F. Horowitz, A. Folch, 3D-printed microfluidics. *Angew. Chem. Int.* **55**(12), 3862–3881 (2016)
- N. Bhattacharjee, A. Urrios, S. Kanga, A. Folch, The upcoming 3D-printing revolution in microfluidics. *Lab on a Chip* **16**(10), 1720–1742 (2016)
- H. Becker, L.E. Locascio, Polymer microfluidics devices. *Talanta* **56**(2), 267–287 (2002)
- M. Brammer, T. Mappes, Modular platforms for optofluidic systems. *Optofluidics* **1**(1), 1–10 (2010)
- M. Bucolo, J. Guo, M. Intaglietta, W. Coltro, Special issue on microfluidics engineering for point-of-care diagnostics. *IEEE Trans. Biomed. Circ. Syst.* **11**(6), 1488–1499 (2017)
- F. Cairone, S. Gagliano, D. Carbone, G. Recca, M. Bucolo, Micro-optofluidic switch realized by 3D printing technology. *Microfluid. Nanofluid.* **20**(4), 1–10 (2016a)
- F. Cairone, S. Gagliano, M. Bucolo, Experimental study on the slug flow in a serpentine microchannel. *Int. J. Exp. Thermal Fluid Sci.* **76**, 34–44 (2016b)
- F. Cairone, D. Mirabella, P.J. Cabrales, M. Intaglietta, M. Bucolo, Quantitative analysis of spatial irregularities in RBCs flows. *Chaos Solitons and Fractals* **115**, 349–355 (2018a)
- F. Cairone, D. Ortiz, P.J. Cabrales, M. Intaglietta, M. Bucolo, Emergent behaviors in RBCs flows in micro-channels using digital particle image velocimetry. *Microvasc. Res.* **116**, 77–86 (2018b)
- S. Camou, H. Fujita, T. Fujii, PDMS 2D optical lens integrated with microfluidic channels: principle and characterization. *Lab Chip* **3**, 40–45 (2003)
- H.N. Chan, Y. Chen, Y. Shu, Y. Chen, Q. Tian, H. Wu, Direct, one-step molding of 3D-printed structures for convenient fabrication of truly 3D PDMS microfluidic chips. *Microfluid. Nanofluid.* **19**(1), 9–18 (2015)
- H.N. Chan, M.J.A. Tan, H. Wu, Point-of-care testing: Applications of 3D printing. *Lab Chip* **17**(16), 2713–2739 (2017)

- D.A. Chang-Yen, R.K. Eich, B.K. Gale, A monolithic PDMS waveguide system fabricated using soft-lithography techniques. *J. Lightwave Technol.* **23**(6), 2088–2093 (2005)
- H. Cong, F.C. Loo, J. Chen, Y. Wang, S.K. Kong, H.P. Ho, Target trapping and *in situ* single-cell genetic marker detection with a focused optical beam. *Biosens Bioelectron.* **133**, 236–242 (2019)
- A. Cossarizza, H.D. Chang, A. Radbruch, M. Akdis, I. Andrä, F. Annunziato, Guidelines for the use of flow cytometry and cell sorting in immunological studies. *Eur. J. Immunol.* **47**(10), 1584–1797 (2017)
- S. Gagliano, G. Stella, M. Bucolo, Real-time detection of slug velocity in microchannels. *Micromachines.* **11**(3), 241 (2020)
- P.C.H. Li, *Microfluidics Lab-on-a-Chip for Chemical and Biological Analysis and Discovery*, p. 94. CRC Taylor and Francis (2006)
- A. Llobera, R. Wilke, S. Buttgenbach, Enhancement of the response of poly(dimethylsiloxane) hollow prisms through air mirrors for absorbance-based sensing. *Talanta* **75**(2), 473–479 (2008)
- J.C. McDonald, G.M. Whitesides, Poly(dimethylsiloxane) as a material for fabricating microfluidic devices. *Acc. Chem. Res.* **35**(7), 491–499 (2002)
- N.P. Macdonald, J.M. Cabot, P. Smejkal, R.M. Guijt, B. Paull, M.C. Breadmore, Comparing microfluidic performance of three-dimensional (3D) printing platform. *Anal. Chem.* **89**(7), 3858–3866 (2017)
- P. Minzioni, R. Osellame, C. Sada, S. Zhao, F.G. Omenetto, K.B. Gylfason, T. Haraldsson, Y. Zhang, A. Ozcan, A. Wax, Roadmap for optofluidics. *J. Optic.* **19**(9) (2017)
- J.M. Ng, I. Gitlin, A.D. Stroock, G.M. Whitesides, Components for integrated poly (dimethylsiloxane) microfluidic systems. *Electrophoresis* **23**(20), 3461–3473 (2007)
- F. Sapuppo, A. Llobera, F. Schembri, M. Intaglietta, V.J. Cadarso, M. Bucolo, A polymeric micro-optical interface for flow monitoring in biomicrofluidics. *Biomicrofluidics* **4**(2), 6258 (2010)
- F. Sapuppo, F. Schembri, L. Fortuna, A. Llobera, M. Bucolo, A polymeric micro-optical system for the spatial monitoring in two-phase microfluidics. *Microfluid. Nanofluid.* **12**, 165 (2012)
- D.I. Walsh, D.S. Kong, S.K. Murthy, P.A. Carr, Enabling microfluidics: From clean rooms to makerspaces. *Trends Biotechnol.* **35**(5), 383–392 (2017)
- G. Weisgrab, A. Ovsianikov, P.F. Costa, Functional 3D printing for microfluidic chips. *Adv. Mater. Technol.* **4**(10), 1900275 (2019)
- A. Yamaguchi, T. Fukuoka, K. Kuroda, R. Hara, Y. Utsumi, Dielectrophoresis-enabled surface enhanced Raman scattering of glycine modified on Au-nanoparticle-decorated polystyrene beads in micro-optofluidic devices. *Colloids Surf. A Physicochem. Eng. Asp.* **507**, 118–123 (2016)
- A.A. Yazdi, A. Popma, W. Wong, T. Nguyen, Y. Pan, J. Xu, 3D printing: An emerging tool for novel microfluidics and lab-on-a-chip applications. *Microfluidics and Nanofluidics* **20**(3), 50 (2016)
- F. Yeshaiahu, L.P. Lee, D. Psaltis, C. Yang, *Optofluidics Fundamentals. Devices and Application*. McGraw-Hill (2010)
- H.T. Zhaoa, Y. Zhang, P.Y. Liu, P.H. Yap, W. Ser, A.Q. Liu, Chemical reaction monitoring via the light focusing in optofluidic. *Waveguides* **280**, 16–23 (2019)

Publisher's note Springer Nature remains neutral with regard to jurisdictional claims in published maps and institutional affiliations.